Comparison of wind tunnel and freestream conditions on the numerical predictions of the flow in a two elements wingsail

Alessandro Fiumara, Nicolas Gourdain, Vincent Chapin, Julien Senter

▶ **To cite this version:**

Alessandro Fiumara, Nicolas Gourdain, Vincent Chapin, Julien Senter. Comparison of wind tunnel and freestream conditions on the numerical predictions of the flow in a two elements wingsail. AAAF 50th Applied Aerodynamics Conference (AERO 2015), Mar 2015, Toulouse, France. pp.1-12. ⟨hal-02168473⟩

HAL Id: hal-02168473

https://hal.science/hal-02168473v1

Submitted on 28 Jun 2019

HAL is a multi-disciplinary open access archive for the deposit and dissemination of scientific research documents, whether they are published or not. The documents may come from teaching and research institutions in France or abroad, or from public or private research centers.

L'archive ouverte pluridisciplinaire **HAL**, est destinée au dépôt et à la diffusion de documents scientifiques de niveau recherche, publiés ou non, émanant des établissements d'enseignement et de recherche français ou étrangers, des laboratoires publics ou privés.

HAL Authorization

Open Archive Toulouse Archive Ouverte (OATAO)

OATAO is an open access repository that collects the work of some Toulouse researchers and makes it freely available over the web where possible.

This is an author's version published in: https://oatao.univ-toulouse.fr/23771

To cite this version :

Fiumara, Alessandro and Gourdain, Nicolas and Chapin, Vincent and Senter, Julien Comparison of wind tunnel and freestream conditions on the numerical predictions of the flow in a two elements wingsail. (2015) In: AAAF 50th Applied Aerodynamics Conference (AERO 2015), 30 March 2015 - 1 April 2015 (Toulouse, France).

Any correspondence concerning this service should be sent to the repository administrator: tech-oatao@listes-diff.inp-toulouse.fr

COMPARISON OF WIND TUNNEL AND FREESTREAM CONDITIONS ON THE NUMERICAL PREDICTIONS OF THE FLOW IN A TWO ELEMENTS WINGSAIL

Alessandro Fiumara[1], Nicolas Gourdain[2], Vincent Chapin[3], Julien Senter[4]

Abstract

This paper is devoted to the study of a 1/20-scale model of wingsail in a wind tunnel environment. This study deals with the methodology to achieve accurate comparisons between numerical and experimental data. A particular care is brought in the numerical simulation to reproduce the wind tunnel effects on the model. The experimental results did not match with preliminary numerical simulations performed in a freestream domain. The reason is that the wind tunnel domain introduces some modifications in the flow field, around the wingsail, especially near the tip. As a consequence, a study has been done first to set the correct configuration to model the real vein conditions. Then numerical simulations based on a RANS approach have been run to study the flow around the wing in the wind tunnel environment, at different operating conditions in terms of inlet flow angles and wingsail cambers. A comparison of the numerical predictions with experimental data established the accuracy of the selected approach. The numerical results were then used to complete the investigations done during the experimental campaign.

[1] PhD student, Assystem and ISAE/DAEP
[2] Professor, Department of Aerodynamics, Energetics and Propulsion, ISAE, University of Toulouse
[3] Associate Professor, Department of Aerodynamics, Energetics and Propulsion, ISAE, University of Toulouse
[4] PhD Engineer, Fluid Dynamics team manager, Assystem France

NOMENCLATURE

α	Angle of attack of the main element
c	Total chord of the wingsail
c1	chord of the main element
δ	Flap deflection angle
C_D	Drag coefficient
C_L	Lift coefficient
H	Mast height
h	Vertical distance from the wing foot
g	Non-dimensional slot width (g/c1)
Re	Reynolds number
Reθ	Momentum thickness Reynolds number
Cp	Pressure coefficient
Sv	Reference area
Cf	Skin friction coefficient
γ	Turbulence intermittency
z^*	Non-dimensional distance (h/H)
q	Cinematic pressure
LWL	Load waterline length

INTRODUCTION

In 2010 the class rule of the America's Cup has introduced the use of foiling boats, the AC 45 & AC 72 (fig. 1), propelled by a rigid wingsail instead of the classical main-sail. The next edition of the competition will be run on AC 45 and the new AC 62, less expensive than the previous model.

	AC 62	AC 72	AC 45
LWL	19 m	22 m	13.5 m
Mast height	32 m	40 m	25.5 m
Wingsail	175 m^2	260 m^2	85 m^2
Hull weight	4300 kg	5900 kg	1400 kg

Tab.1: dimensions of the AC 62, AC 72 and AC 45

The rigid wingsail is composed of two symmetric wings with a slot between them to control the sail camber on starboard and port tack (fig. 1). It allows achieving high performance in term of power and lift to drag ratio compared to a conventional soft mainsail but the entire "sailing envelope" is largely unknown. Particularly at near stall conditions, the aerodynamic behavior of the wing is still not well understood. This lack prevents teams to have a global knowledge of the behavior of the wingsail during the navigation. Capsizes of the American and the Swedish teams have shown the difficulty to maneuver the wing without causing stability problems. However, the possibility of its usefulness even in domains different from the sporting one has recently rekindled the interest for new concept design of wind driven vessel in the era of low carbon society [1] [2].

To have a better understanding of the flow physics around such a wingsail, a wind tunnel campaign was set on 1/20 scale model. At the same time numerical studies were carried on the same geometry in freestream conditions.

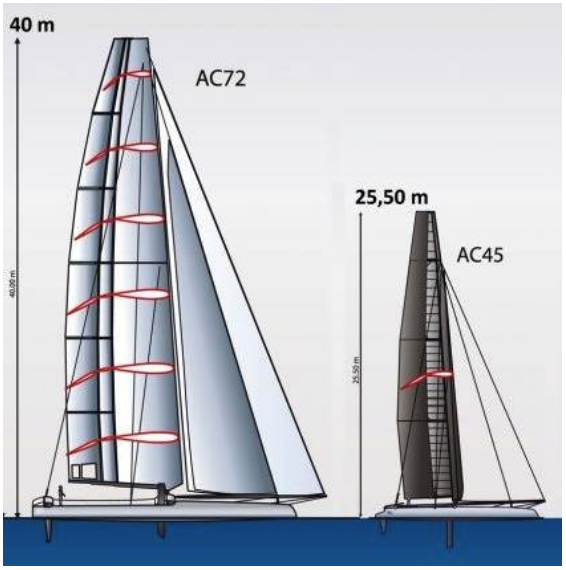

Figure 1: AC45 & AC72

Unfortunately such a numerical approach was responsible for major discrepancies regarding the wingsail performance, compared to experimental measurements. As it will be shown in this paper, the reason is that numerical and experimental campaigns were considering two different configurations, i.e. the experimental results are obtained inside a wind tunnel while the numerical solution is computed in a feestream domain without constraints imposed by the wind tunnel walls. Usually a wind tunnel has its own flow field that interacts with the flow around the tested model. Hence it is important to estimate and understand the effects of these interactions on the studied geometry.

The geometry considered in this paper is a particular model of bi-element profile, representative of a wingsail. This configuration is also relevant to the typical high-lift geometries encountered for aeronautical wings [3][4]. The study reported in this paper has two objectives:

- Understand the interactions between the wing and the wind tunnel and analyze their effects on the flow field, especially at near stall conditions.

- Propose a method to take into account for the wind tunnel effects in numerical simulations;

The first part of the paper presents the wingsail geometry and operating conditions. Three different strategies are then detailed in a second part to numerically reproduce the flow in the wind tunnel. Then the wingsail is added in the numerical simulations to investigate the effect of the wind tunnel on the flow around the profile. Finally, the last part of the paper deals with a comparison of the flow with and without the presence of the wind tunnel around the wingsail.

1. GEOMETRY AND NUMERICAL PARAMETERS

The geometry chosen is a simplified configuration of a 1/20 scale AC72's rigid multi-elements wingsail (fig. 2). It is a two elements swept wing, composed by a main element and a flap, whose chord ratio is 0.5. The slot between the two elements is constant along the wingspan; the flap can be deflected at different angles with respect to the main element in a way to modify the camber of the global profile of the wing.

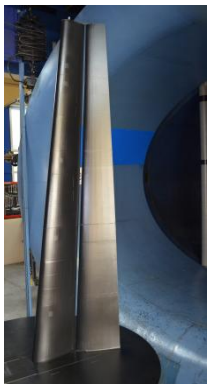

H	1.80 m
Sv	0.657 m^2
Re_{root}	$6.4 \cdot 10^5$
Re_{tip}	$2.9 \cdot 10^5$

Figure 2: photo of the wing model and its parameters

The model of the wingsail has been studied with URANS numerical simulations in order to understand the physics of its flowfield at different angles of attack and camber. The objective was to obtain the polar of a low cambered and a high cambered configuration of the wing.
Simulations have been done with Star-CCM+ 8.04 using an unsteady RANS approach. The two equations k-ω SST model is used to model the effects of turbulence. The laminar to turbulent transition of boundary layers is modeled by adding two transport equations for the intermittency factor γ and the Re_θ quantity as suggested in [5]. The computational domain in freestream conditions is presented in fig. 3. A velocity inlet condition is imposed at the inlet, windward, leeward and ceiling walls; at the outlet a pressure condition is used while a symmetric condition is applied for the bottom wall.

The global attitude of the wing is dependent to the wingsail cambers δ, especially at near stall conditions. Figure 4 shows the lift coefficient C_L with respect to the inlet flow angle α, at two different camber positions.

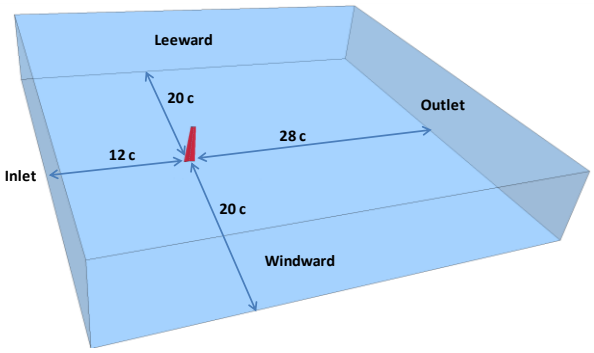

Figure 3: computational domain with wingsail

The low cambered configuration has a canonical evolution in C_L with a first linear increase and a final loss in C_L once overtaken the α stall. The trend of the same curve for the high cambered configuration is more complicated: after a first loss of C_L, corresponding to the stall of the flap surface only, the C_L remains quite constant up to the final α stall where the entire wing is stalled. This phenomenon of multistep stall is characteristics of the multielement airfoils, already described by Biber in 1983 [6]. In fact, a variation of the wing camber modifies the intensity of the jet induced by the slot between the main element and the flap. This jet, which flows from the pressure side to the suction side, is thus partly responsible for the different behavior observed in figure 4.

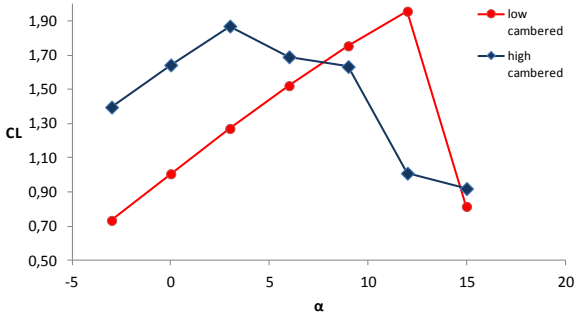

Figure 4: C_L/α for the wingsail in freestream in two different cambered configurations.

The jet is entrained by the wake of the main element that modifies its direction. In the low cambered configuration the flap imposes a moderate deflection. So the jet of the slot impacts directly on the upper surface of the flap "pushing down" its boundary layer. In this way the boundary layer itself is stabilized by the jet

delaying the stall of the flap. The two elements of the wing stall at the same time as a simple element wing.

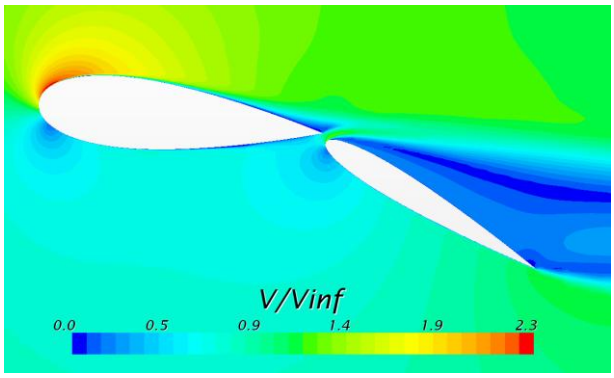

Figure 5: barrier effect of the jet of the slot for high cambered configuration

In the high cambered configuration, on the contrary, the flap is positioned farther from middle line of the main element and thus from the wake of the main. The jet of the slot is no longer in contact with the upper surface of the flap, as in the previous case. The more α increases the more the jet goes far from the flap surface creating a barrier that divides the flow of the main element by the flow of the flap (fig. 5). The two elements in this case can be considered as independent; the flap stalls earlier because of its angle of deflection. The main element stalls only in a second time.
Furthermore the stall of the flap involves only the mid-high part of the flap itself. This is due to the Re reduction moving tip ward because of the chord reduction. The Re in the higher sections of the wing is lower than that one the lowest sections. Hence the flow on the higher part of the flap detaches more rapidly in comparison to the low sections. This phenomenon can be observed in fig. 6.

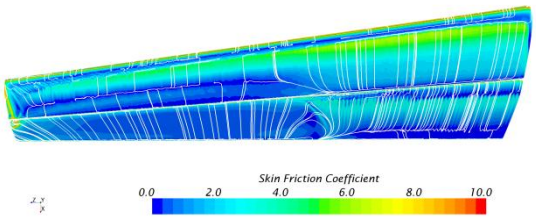

Figure 6: skin friction on the suction surface of the wing in freestream at alpha=6°

During the experimental tests the same stall phenomena were observed. Nevertheless the angles of attack at which the stalls take place moved toward lower values; at the same time the modulus of the C_L have a deficit of 0.4 with respect to the simulations of the wing in freestream domain. The role of the wind tunnel walls has been investigated to analyze these differences.

2. WIND TUNNEL MODELING

The S4 wind tunnel

The wind tunnel chosen for the experimental tests is the S4 facility, owned by ISAE in Toulouse. It is a wind tunnel with an open test section of elliptical shape and dimensions of 3m×2m (fig. 7a).

(a)

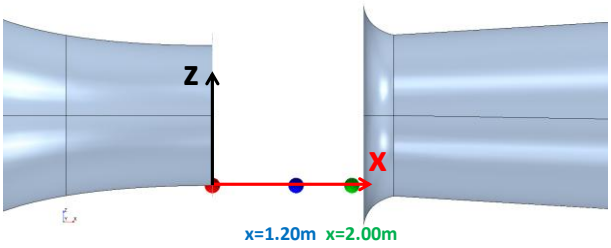

(b)

Figure 7: (a) view of the open vein in the S4 facility; (b) wind tunnel cartesian system.

The wind is generated by the aspiration operated by three engines of 90 kW each located at the end of the divergent. The maximal speed of the flow in the vein is 42 m/s. To prevent problems of low frequencies oscillations of the flow in the vein, a gap was created on the diffuser surface not far from its intake. In this manner part of the flow in the diffuser is spilled off by the gap dumping the oscillations. The flow spilled off returns at the diffuser intake by an exterior recirculation.

Geometry

The numerical reproduction of the wind tunnel geometry has introduced some difficulties concerning the way to close the vein domain without modifying the global flow field at its interior. Three different closures of the domain have been tested:

- By doing a simple homothesis from the convergent to the diffuser (fig. 8a);
- By adding the test room containing the vein (fig. 8b);

- By adding the test room and also the recovering flow from the diffuser to the exit of the vein (fig. 8c).

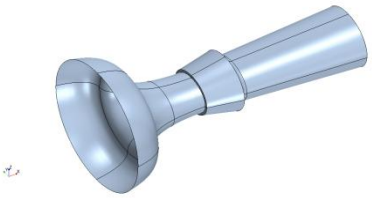

(a)

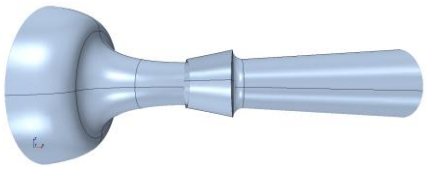

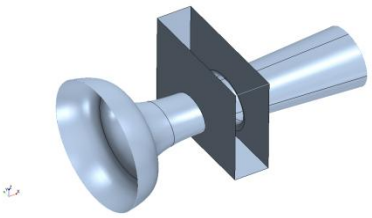

(b)

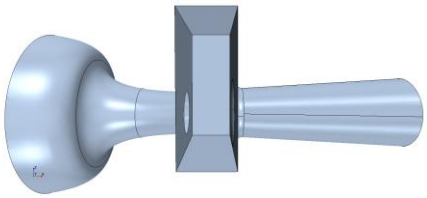

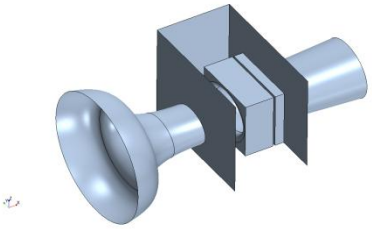

(c)

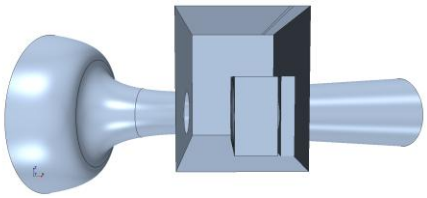

Figure 8: numerical geometries of the wind tunnel: (a) S4-0, (b) S4-1, (c) S4-2

The three geometries are named respectively as S4-0, S4-1, S4-2. These have been analyzed with numerical simulations without profile (i.e. the vein is empty). The cinematic pressure distributions of the vein of the three configurations have been compared to the measured distribution of the real wind tunnel.
The coordinate system for the vein has the origin at the exit of the convergent, in the lower part of the minor axis of the ellipse (fig. 7b). The x axis of the coordinate systems is perpendicular to the exit section of the convergent (streamwise direction); the z axis lies on the minor axis of the ellipse with upward direction; the y axis oriented to complete cartesian system.

Simulations

The simulations for the wind tunnel configurations analysis were all run with Star-CCM+ 9.02. Domains have been meshed with polyhedral and prism layers at the walls. The number of cells ranges between 0.45M cells for the simplest S4-0 to 1.4M for the more complex S4-2. The extra number of cells is due to the extra volumes introduced in the S4-2. Two pressure outlet conditions have been imposed at the intake of the convergent and the exit of the diffuser in order to reproduce the aspiration procured by the engines. The difference of the pressures intake-outlet was set in order to obtain a velocity of 20 m/s on the two points, at the exit of the convergent, where the pitot tubes are located in the real wind tunnel.
The simulations converge after 2000 iterations and 2 hours of calculations on 4 processors.

Results

The distributions of the cinematic pressure (q) inside the vein of the wind tunnel were compared with the data of the real wind tunnel. A line probe was placed in the middle of the vein (y=0, z=1.0 m) ranging from the exit of the convergent to the entry of the diffuser in the x direction. Probes in the y direction, ranging on the entire major axis of the ellipse, were placed at three different sections of the vein: at the exit of the convergent (x=0), on the axe of fixation of the model (x=1.2 m) and at the entry of the diffuser (x=2.0 m). On the same sections, probes in z direction were placed, ranging on the entire minor axis of the ellipse.
The cinematic pressure was normalized with respect to the value of q0 i.e. the cinematic pressure in the center of the vein (x=1.2 m, y=0, z=1.0 m). In the **x direction** the real S4 has a constant distribution in q/q0 up to x=1.5 m for then decreasing of the 4% of its reference value (fig.9). The numerical S4-1 and S4-2 are similar to the real distribution with some differences. The S4-1 has a little increase in velocity in the first part of the vein for then decreasing to values smaller than the real ones. The S4-2 has a more constant distribution all along the vein and particularly at the exit of the vein where even the real wind tunnel presents a loss in

velocity. The S4-0, the simplest configuration, has the most different distribution from the real values.

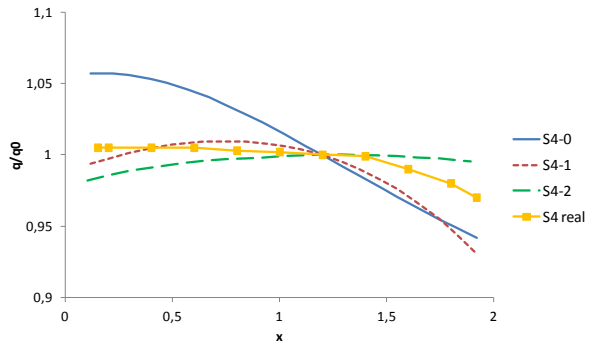

Figure 9: comparisons of the q/q0 of the vein in the x direction

	Pressure gradient dq/dx (Pa/m)		
	S4-0	S4-1	S4-2
0<x<0.5	-3.00	7.39	4.49
0.5<x<1.2	-12.75	-3.54	1.26
1.2<x<2.0	-13.16	-21.7	-1.27

Tab.2

On the model location along x axis (x=1.20m) the cinematic pressure gradient in the **y direction**, is smaller than the one in x direction with nearly 6.29 Pa/m for S4-1 and nearly 0 Pa/m for S4-0, S4-2 and S4-real (fig.10). At the same time the S4-1 and S4-2 manages to keep a good value in velocity even at the limits of the vein while the S4-0 has important effects of contraction of the vein. Always on the model location among x-axis (x=1.20m) the pressure gradient in the z direction is smaller than in x direction, of the same order than in y direction. S4-0 presents a dissymmetry with dq/dz=-4.95 Pa/m with a nominal velocity (q/q0=1) for 0<z<0.5 and a higher velocity (q/q0=1.01) for 0.5<z<1.

The most important differences can be found at the end of the vein, on the section of the entry of the diffuser (fig. 11). The S4-0 has the worst modelisation in this case having an error of about 4% compared with the real distribution and a loss in velocity of the flow. The same error can be found for the S4-1 but only in the middle part of the vein while on the vein limits there is a global recuperation in velocity.

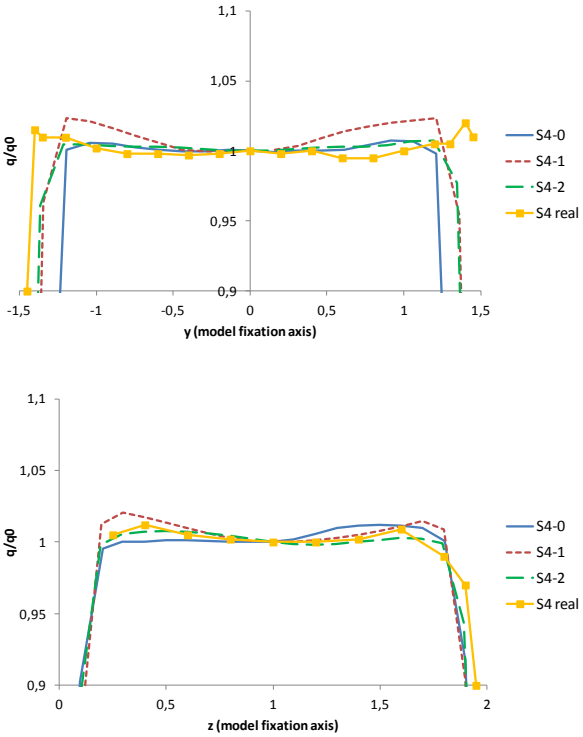

Figure 10: comparisons of the q/q0 distribution on the model fixation section in the y and z direction

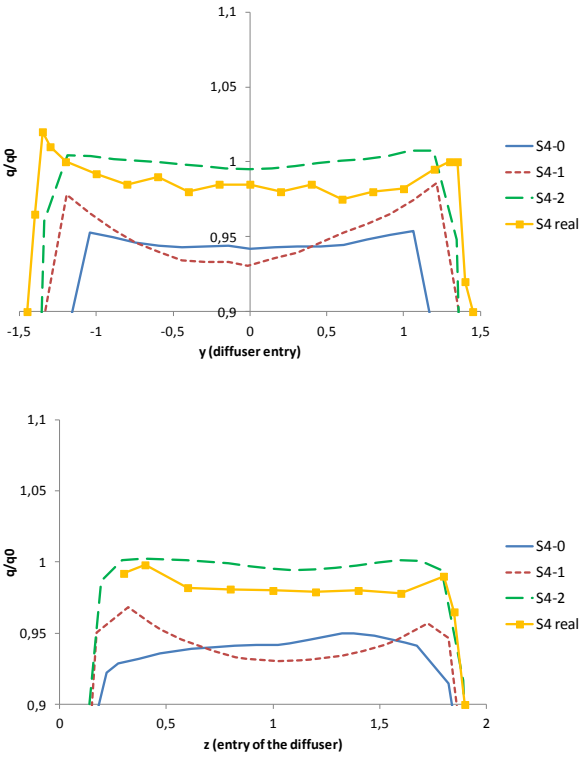

Figure 11: comparisons of the q/q0 distribution on the section at the entry of the diffuser, in the y and z direction

The best reproduction is obtained with the S4-2 model. The loss in velocity along **x-axis** of the wind tunnel is not reproduced, but the error is less than 2% and the global distribution is very similar to the real one with a very low adverse pressure gradient.

The S4-2 model is the only numerical model that does not introduce a fictive adverse pressure gradient in the vein and globally it reproduces the same characteristics of the real vein. The S4-1 may be an alternative but it introduces an adverse pressure gradient in the rear part from the middle of the vein to the diffuser (Tab.2). The S4-0 can reproduce the vein effect particularly in the section of the model fixation axis. However, it introduces a strong adverse pressure gradient three or four times higher than the one in the real S4. This may introduce non physical behavior of the flow around the model.

3. WINGSAIL IN WIND TUNNEL DOMAIN

Once analyzed the three numerical geometries of the wind tunnel, simulations of the wingsail inside the three geometries have been run.
The aim here is to quantify the interactions between the wing and the wind tunnel domain in these three numerical models of the wind tunnel.

Geometry and mesh

The wingsail was considered in its high cambered configuration, the most critical configuration because of its high sensitivity to environment conditions. It was located vertically in the wind tunnel vein in correspondence of the model fixation axis, at a zero angle of attack. The interface disk at the wing foot, used during the experimental campaign, is also modeled.
The domain was meshed with polyhedra and wall prism layers. The mesh was strongly refined on the wing surface using a max cell size of 2.0 mm and a minimum one of 0.2 mm. This refinement was necessary for the correct operation of the transition model used for the simulations. On the wing walls 20 prism layers have been imposed with the near wall layer dimension of $7 \cdot 10^{-6}$ m. The y+ on the wing varies from 0.2 to 0.6.
The cell refinement on the wind tunnel walls is coarser. Refinement was also imposed on the mixing layer zones of the wind tunnel. The global mesh of each of the three configurations counts about 32 millions cells.
The limit conditions for inlet and outlet of the wind tunnel were kept the same as the empty wind tunnel simulations.

Results

In this case the analysis was focused on the characteristics of the flow over the wing. Nevertheless in the three simulations the flow velocity in the vein was not rigorously identical: for the S4-2 configuration the target speed of 20 m/s is achieved, while for S4-0 and S4-1 the velocity is 18 m/s and 18.25 m/s, respectively. This reduction of the velocity in the test section only modify the Re values by less than 10%, thus the results on the different wing configurations remain comparable. The values found for C_L are very similar and have a discrepancy of about 10% with the experimental value (Tab.3).

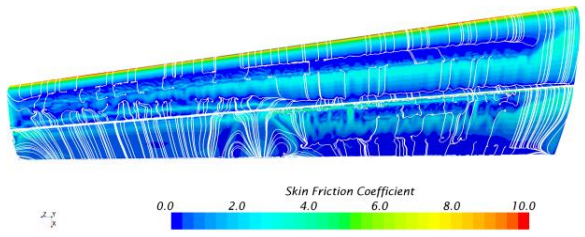

(a)

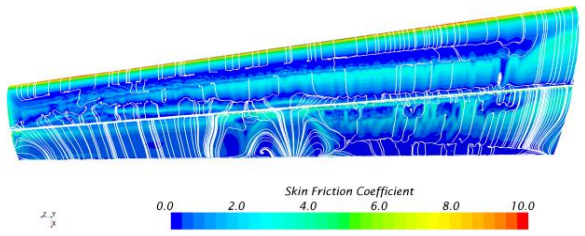

(b)

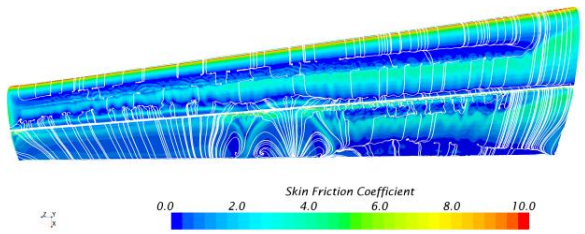

(c)

Figure 12: skin friction on the suction surface of the wing with wall streamlines. (a) Wing in S4-0, (b) wing in S4-1, (c) wing in S4-2.

The global correspondence of the solutions of the three configurations is confirmed by the similarity of the pressure coefficient Cp distributions (fig. 14) over the reference sections of the wing, i.e. z*=0.25, z*=0.5, z*=0.75. For the z*=0.5 section there is a difference on the value of Cp between S4-0 and S4-1/S4-2; this difference is caused by the movement upward of the crossflow transition zone for the S4-0 case.
In figure 12 the time-averaged skin friction distributions over the wing are reported. In the three simulations the flow shape is almost similar. On the main element of the wing the flow is laminar in the expansion zone of the profile for then forming a laminar bubble near the minimum pressure point. In the recompression zone the

flow reattaches and become turbulent. Near the trailing edge the turbulent flow detaches from the wing surface. On the flap the phenomena are a little bit more complicated. In the lower part of the flap in fact the flow has a structure similar to that one already seen for the main element. On the contrary the higher part sees a completely detached flow all along its chord. In the middle sections of the flap there is a "crossflow transition" region between the lower part, where the flow is attached and laminar, and the higher part, where the flow is detached and turbulent. This transition zone presents strong 3D phenomena with contra rotating vortex. This same structure of the flow has been observed in the experimental tests (fig. 13). In figure 13 it could be seen how the gap between the two elements is not constant along the wingspan but is larger at ¾ of the span. This is due to the deformation of the components of the real model that presents some inequalities in comparison with the numerical wing. These deformations will be taken into account for the future numerical analyses of the wing.

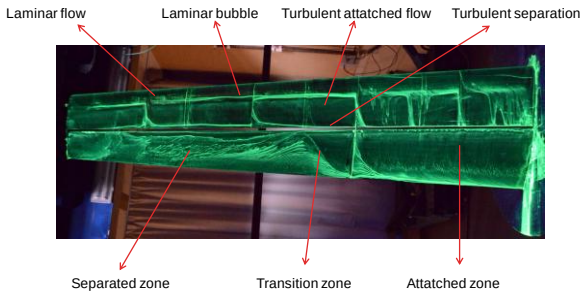

Figure 13: surface oil flow visualization over the wing during the experimental tests

The difference in the three configurations concerns the location on the wingspan of the transition zone between the high and the low parts. In the S4-0 configuration this zone is located tip ward of the 15% of the chord in comparison with the S4-1 and S4-2 configurations. At the same time the S4-0 has also the smaller crossflow transition zone. On the sections where the flow on the flap is detached, modifications can be noticed also on the main element.

Particularly the flow tends to separate earlier of about 8% of the main element chord from the main element surface. This is observed mainly for S4-0 and S4-1 configurations. In the S4-2 case the constant distribution in pressure in the streamwise direction helps to maintain the flow attached, contrary to S4-0 and S4-1 cases where an adverse pressure gradient exists.

	S4-0	S4-1	S4-2	S4 real
C_L	1.11	1.09	1.09	1.21

Tab.3

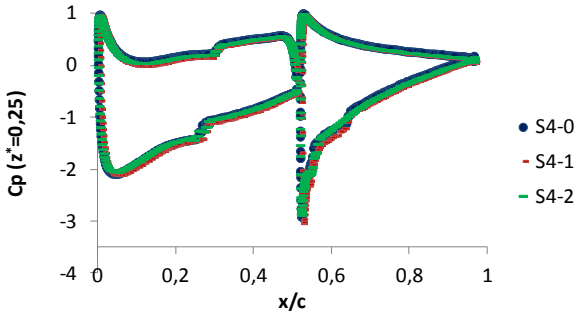

(a)

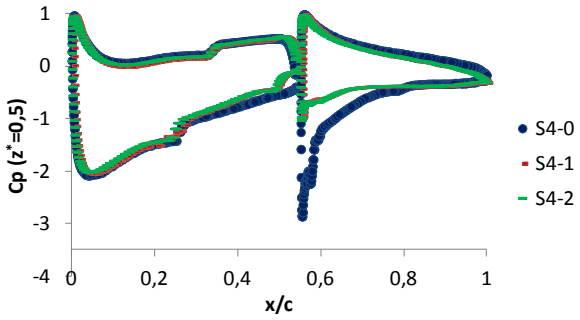

(b)

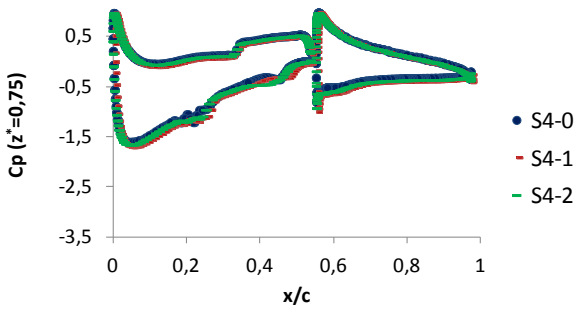

(c)

Figure 14: Cp distribution of the wing in the three wind tunnel modelisations over three different wing sections: (a) z^*=0.25, (b) z^*=0.5, (c) z^*=0.75

4. WIND TUNNEL AND FREESTREAM COMPARISON

The high cambered wing

The flow patterns around the wing in the wind tunnel domain have been compared with the flow around the wing in the freestream domain. As noticed in fig. 15 the flow is modified by the presence of the wind tunnel. In freestream conditions the flow does not change along the wingspan: on the main element the flow is laminar in the expansion zone of the profile for then forming a laminar bubble. The transition to turbulent flow appears in the recompression zone where the flow rest attached until the trailing edge. On the flap the flow is attached until 75% of the chord on the sections up to 75% of the

wingspan; then the detachment line moves toward the 50% of the chord. This is due to a Re effect caused by the reduction of the chord in the high sections of the wing.

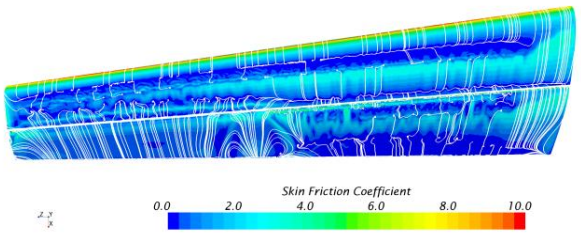

(a)

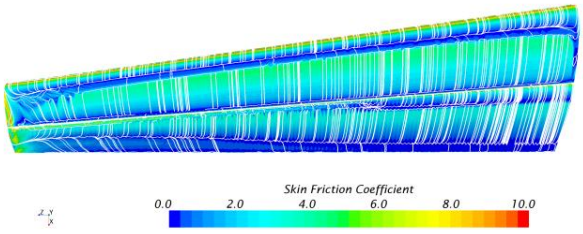

(b)

Figure 15: skin friction on the suction surface of the wing in S4-0 (a) and in freestream (b)

In these conditions one can say that the wind tunnel tests cannot reproduce the flow field on a wing in freestream conditions. However, figure 6 shows that the wing in freestream conditions at an angle of attack of 6° is similar to the flow field in the wind tunnel at zero angle of attack (fig. 15a). Hence the effect of the wind tunnel is to increase the angle of attack felt by the wing. Watching at the CL/α curve for the freestream case (fig. 4), the wing in the wind tunnel could be located after the first loss in C_L, i.e. after the stall on the flap. Nevertheless the value of the C_L of the wing in freestream after the first stall is about 1.6 while the wing in the wind tunnel has a C_L of 1.11. Thus the anticipated stall cannot completely explain the difference in C_L.
To go further in the analysis of the interaction between the wing and the wind tunnel the deflection angles of the flow have been analyzed on both the freestream and the wind tunnel configurations. Line probes in the x direction (streamwise) were located at y=0 and z^*=0.25, 0.5, 0.75, 1.05. Two deviation angles have been indentified and calculated:

- φ: deviation angle between y and x
- ψ: deviation angle between z and x.

The graphics of these angles have been reported in fig. 16 and 18. The comparison between the two graphs indicates that the global effect of the wind tunnel is to straighten the flow reducing the local angle of attack felt by the wing. This difference amounts to about 5°. This straighten effect is caused by the interaction of the flow into the vein with the mixing layers that divide that the flow at the interior of the vein from the exterior flow at rest. The mixing layers represent an iso-pressure limit condition that is applied on the entire border of the vein; this condition balances the difference of pressure between suction and pressure side of the wing, reducing the flow deviation on the wing itself. This effect is further increased by the presence of the diffuser walls downstream of the wing. In fact, the wake of the wing is deviated toward the pressure side due to its cambered configuration (fig.17). Nevertheless the wake cannot evolve freely but it is straighten by the walls of the diffuser. This perturbation is felt by the upstream flow so that the flow deviation appears reduced in comparison to the freestream case where the wake has no constraints.

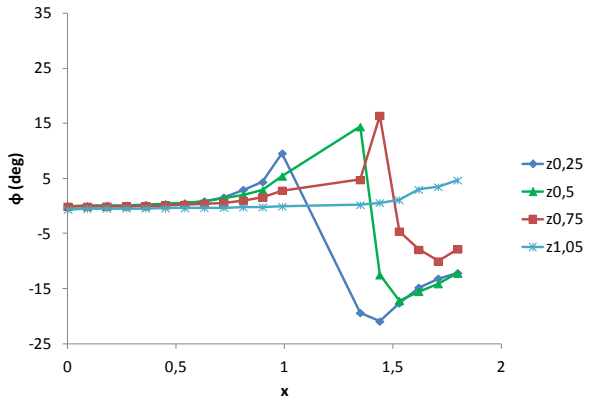

(a)

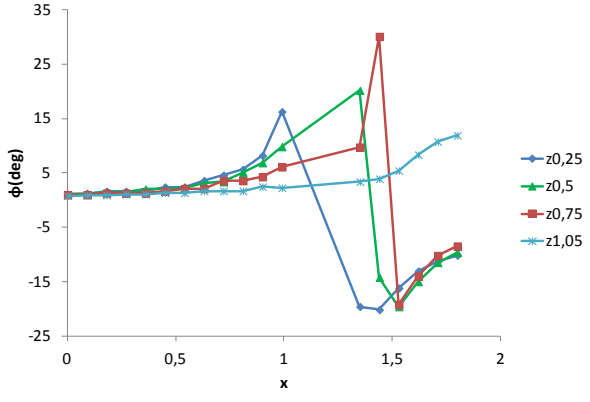

(b)

Figure 16: φ distribution in the S4-0 (a) and in the windtunnel (b)

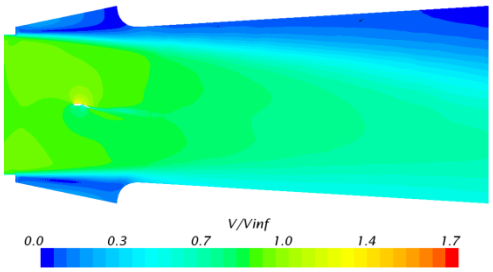

Figure 17: flow deviation inside the diffuser of the wind tunnel caused by the presence of the wing

The differences in ψ between the wind tunnel and freestream configurations are lower than the differences in phi. In the two lowest sections, z^*=0.25 and z^*=0.5, the psi angle is negative in the wind tunnel and positive for the freestream domain. The divergent shape of the vein provokes this flow deviation. Furthermore the largest and important deviation is observed on the wing tip. Here the difference in deviation varies from 2° to 4° with the freestream configuration where the deviation angles are near to zero.
On a swept wing the flow field has a transversal component going from the root to the wingtip and forming a transversal boundary layer [7]. In the wind tunnel, having an increase of the ψ angle, this transversal component is accentuated. The transversal boundary layer develops faster than in the precedent case giving origin to perturbations that worsen the stability of the flow. This kind of instability is known as "crossflow instability" [8] and it is characteristic of the swept wings where the flow is highly 3D.
Furthermore the flow on the upper part of the flap is sensitive to small perturbations that can cause its detachment from the wing surface. On the wing in the freestream case, this perturbation is due to the streamwise adverse pressure gradient that increases with the angle of attack. When the stalled angle of attack of the flap is overtaken, the flow detaches from the upper surface of the flap. In the wind tunnel the detachment is generated by perturbations that act in the crossflow and not in the streamwise direction. This perturbation causes the separation of the flow in the upper part of the flap.

To resume the ψ deviation introduced by the wind tunnel perturbs the flow on the upper part of the flap provoking its separation. This is related to the first loss in C_L on the C_L/α curve of the wing. This explains the similitude between the flow field in freestream conditions at 6° of angle of attack and the wing in the wind tunnel at 0°. The further loss in C_L is on the contrary due to the effect of the wind tunnel to straighten the flow in the vein; the wing in the wind tunnel see a smaller angle of attack than that one see by the same wing in freestream.

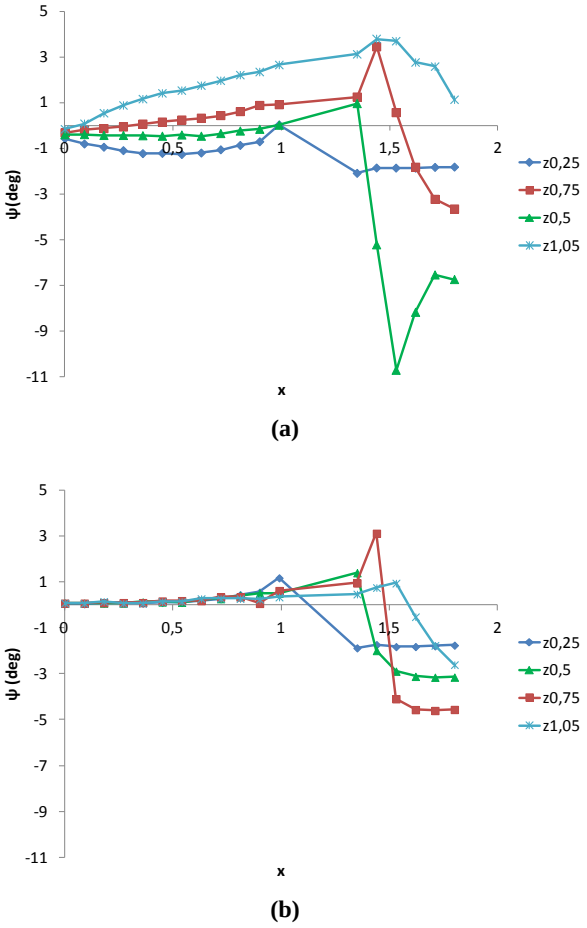

Figure 18: ψ distribution in the S4-0 (a) and in the windtunnel (b)

The low cambered wing

Most part of the study deal with the wing in its high cambered configuration, the most sensible to the exterior perturbations. However some analyses have been effectuated even on the low cambered configuration of the wing to verify its behavior with the wind tunnel interactions.
The C_L evaluates by numerical and experimental means are comparable with a difference of 0.04. The C_L values found for the wing inside the wind tunnel are of 0.2 with respect to the value for the freestream case (Tab.4).
The flow field of the wing in freestream and inside the wind tunnel does not show the strong modifications that had been observed on the high cambered case. Both in free stream and in wind tunnel the flow on the wing has the same structure (fig. 19): on the main element the flow is laminar near the leading edge, forming a laminar bubble in the minimum pressure zone of the profile. Then the flow becomes turbulent separating near the T.E. On the flap the flow has the same characteristics as the main element with the separation point located near the trailing edge on the entire wingspan. Some differences can be noticed only at the wingroot, where in the wind tunnel simulation there is the interface disk,

and at the wingtip where the border effects of the vein begin to be felt.
The low cambered wing did not present modifications in the stall angle of attack with a difference of only 0.5 degrees between the experimental data and the free stream numerical simulation. Hence the loss in C_L in the wind tunnel depends only on the straighten effect introduced by the wind tunnel domain on the flow but secondary phenomena on interference are not observed.
The experimental results on the low cambered configuration on the wing are directly representative of the physics phenomena on the wing in freestream.

	Freestream	S4-0	S4-real
C_L	1.00	0.82	0.78

Tab.4

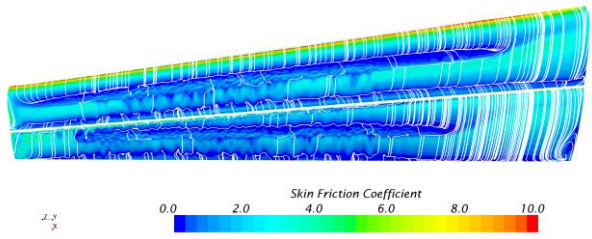

(a)

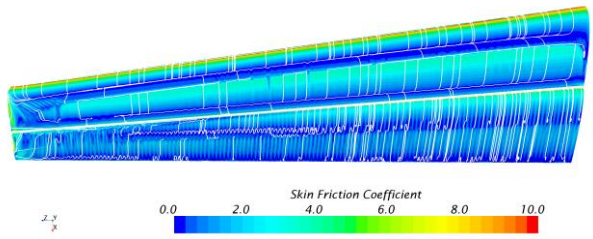

(b)

Figure 19: skin friction and streamlines representations on the wing in S4-0 (a) and in freestream (b)

5. CONCLUSIONS

Jointly with the experimental campaign, numerical simulations have been run on a 1/20 scale wingsail in freestream conditions, as it is useful to clearly indentify similarities and differences between simulations and experiments depending on the way wind tunnel configuration is taken into account. Nevertheless the predictions of the numerical simulations in open conditions do not match experimental measurements regarding the flow patterns along the wingspan and the stall angle. This is particularly true for the wing in its high cambered configuration while the low cambered one the differences that can be noticed are not so important. The reason to explain these discrepancies is that the presence of the wind tunnel walls modifies the flow field around the wingsail.

A new numerical campaign was set taking into account the wind tunnel domain. Because of the open test section of the wind tunnel the numerical domain had to be closed. Three different configurations with different closures have been modeled, without the wing in the vein. The first model uses a simple homothesis to close the domain while the second and the third one reproduce the test room. The third model reproduces also the recirculating flow from the diffuser to the vein. Simulations were run on the empty wind tunnel domain and the characteristics of the flow in the vein have been compared with the real wind tunnel data. The three numerical models gave results in good agreement with the measured velocity profiles in the vein. However the first and second models overpredict the adverse pressure gradient in the streamwise direction, on the rear part of the vein. The third model is able to reproduce a flat pressure gradient as in the experiments.

A last numerical campaign was performed, after adding the wingsail in its high cambered configuration inside the wind tunnel. The velocity of the flow was set at 20 m/s. The flow field remains similar on the three models with the flow attached on the lower part of the flap and detached on the higher part. In the first model this transition zone on the flap moves tip ward and it appears smallest than the other two wind tunnel configurations. In all cases, the C_L values have a discrepancy less than 10% compared to the experimental tests.

The numerical simulation in wind tunnel was then compared with the freestream conditions to better understand the effects of the wind tunnel interactions on the flow field. In the freestream case, the higher part of the flap does not stall. At the same time the lift coefficient C_L in freestream conditions is of 0.4 higher than in the wind tunnel. By an analysis of the deviation angles of the flow both in freestream and in the wind tunnel it emerges the straighten effect, on the local angle of attack, of the wind tunnel on the flow. This explains part of the loss in C_L. The flow separation on a portion of the flap is on the contrary caused by the deflection of the flow upward in the mid-up section of the wing and downward in the mid_down section. This crossflow deviation, in the root-tip direction, perturbs the flow generating “crossflow instabilities” on the higher part of the flap, where the flow is less stable. This phenomenon causes the separation of the flow on this part of the flap provoking a further loss in C_L.

For the low cambered configuration a weak loss in C_L can be observed for the wing tunnel domain. In this case the wind tunnel interactions with the wing influences only the streamwise deviation of the flow that explains the loss in Cl. Further phenomena of interactions are not observed. Even the flowfield structure in the freestream and in the wind tunnel shows the same characteristics.

6. PERSPECTIVES

This study represents the first step for the comprehension of the aerodynamic phenomena appearing on a bi-element wingsail. The analysis of the interactions existing with the wind tunnel walls will allow transposing the experimental data to the configuration of the wing in the freestream domain. Further numerical simulation will be carried on taking into account the deformations that the real model has shown during the wind tunnel tests. Further analyses will be effectuated to deeper investigate the jet of the gap between the two elements and its influence on the stall of the wingsail.

ACNOWLEDGEMENTS

This research was supported in part by ASSYSTEM France, which kindly provided PhD funding. Particular thanks to Laurent Neau, manager of the Flight Physics department of Assystem France, who made possible the creation of this PhD project on the wingsails.

REFERENCES

1. Nakashima, T., Yamashita, Y., Nihei, Y. & Li Q. (2012), "A Basic Study for Propulsive Performance Prediction of a Cascade of Wingsails Considering Their Aerodynamic Interaction", Proceeding of the 2*1th International Offshore and Polar Engineering Conference*, Hawaï, June 2011.
2. Jo, Y., Lee, H. & Choi S. (2013), "Aerodynamic Design Optimization of Wing-Sails", 3*1th AIAA Applied Aerodynamics Conference*, San Diego, June 2013.
3. 1st AIAA CFD High Lift Prediction Workshop (HiLiftPW-1) - 2-Day Workshop June 26-27 2010, Chicago, IL
4. 2nd AIAA CFD High Lift Prediction Workshop (HiLiftPW-2) - 2-Day Workshop - June 22-23 2013, San Diego CA
5. Malan, P., Suluksna, K. & Juntasaro, E. (2009), "Calibrating the γ-Reθ Transition Model for Commercial CFD", *47th AIAA Aerospace Science Meeting*, Jan 2009.
6. Biber, K., Zumwalt, G.W., (1992), "Experimental Studies of a two-element airfoil with large separation", AIAA paper 92-0267, Reno 1992.
7. Sabetta, F., "Gasdinamica", ch. 8 pag.154, Casa Editrice Università La Sapienza, Roma.
8. Saric, W.S., Reed, H.L., White, E.B. (2013), "Stability and transition of three-dimensional boundary layers", Annual Review of Fluid Mech., Vol. 35, 413-440, Jan 2003.